

COMPACT JOSEPHSON φ -JUNCTIONS

S. V. Bakurskiy^{1,2}, N. V. Klenov^{1,4}, I. I. Soloviev^{1,3}, A. S. Sidorenko^{5,6},
M.Yu. Kupriyanov^{1,2}, A.A. Golubov^{1,7}

¹*Lomonosov Moscow State University, Skobeltsyn Institute of Nuclear Physics, 119991, Moscow, Russia*

²*Moscow Institute of Physics and Technology, State University, Dolgoprudny, Moscow region, Russia*

³*Lomonosov Moscow State University, Physics Faculty, 119991, Moscow, Russia*

⁴*N. L. Dukhov All-Russia Research Institute of Automatics, 127055, Moscow, Russia*

⁵*Institute of Electronic Engineering and Nanotechnologies ASM, MD-2028 Kishinev, Moldova*

⁶*Institut für Physik, Universität Augsburg, D-86159 Augsburg, Germany*
Faculty of Science and Technology and MESA+ Institute for Nanotechnology, University of Twente, 7500 AE Enschede, The Netherlands

Abstract: This chapter is devoted to the study of controllable proximity effects in superconductors (S), both in terms of fundamental aspects and applications. As a part of the work theoretical description was suggested for a number of structures with superconducting electrodes and multiple interlayers with new physics related to the proximity effect and nanoscale φ -junctions. They are Josephson structures with the phase of the ground state φ_g , $0 < \varphi_g < \pi$. φ -junctions can be created on the basis of longitudinally oriented normal metal (N) and ferromagnetics (F) layers between superconducting electrodes. Under certain conditions, the amplitude of the first harmonic in the current-phase relation (CPR) is relatively small due to F-layer. The coupling across N-layer provides negative sign of the second harmonic. To derive a quantitative criteria for realization of a φ -junction we have solved two-dimensional boundary-value problem in the frame of Usadel equations for overlap and ramp geometries of different structures with NF-bilayer. This chapter is focused on different geometries of nanoscale φ -structures of the size much less than Josephson penetration depth λ_J . At the same time φ -state cannot be realized in conventional SNS and SFS sandwiches. Proximity effect between N and F layer limits minimal possible size of φ -junction. In the case of smaller junctions, NF-bilayer becomes almost homogeneous, φ -state is prohibited and junction exists in 0- or π -state. The conditions for realization of φ -junctions in ramp-type S-NF-S, overlap-type SFN-FN-NFS and RTO-type SN-FN-NS geometries are discussed in the Chapter. It is shown that RTO-type SN-FN-NS geometry is most suitable for practical realization. It is also shown in this chapter, that the parameter range of φ -state existence can be sufficiently broadened. It allows to realize φ - Josephson junctions using up-to-date technology. By varying the

temperature, we can slightly shift the region of $0-\pi$ transition and and, consequently, we can control the mentioned phase of the ground state. Furthermore, sensitivity of the ground state to an electron distribution function permits applications of φ -junctions as small-scale self-biasing single-photon detectors. Moreover these junctions are controllable and have degenerate ground states $+\varphi$ and $-\varphi$, providing necessary condition for so-called “silent” quantum bits.

Key words: Superconductivity, Magnetism, Josephson Junction, Current-phase Relation (CPR), Josephson Memory, φ - Junction.

1. INTRODUCTION

In recent years the development of superconducting (S) electronics is rapidly growing field [1]. Energy efficiency and high characteristic frequencies of superconductive devices may potentially provide significant benefit compared to other proposals of future electronics circuits. The main direction of this field is the development of controllable superconducting devices and memory elements. The one of the possible ways to control properties of superconducting structures is the implementation of ferromagnetic layers in Josephson junctions [2-12]. There are a lot of different proposals and concepts in this field.

It took a long time before the first experimental observation of coupling even through single ferromagnet (F) layer [13]. This problem was solved with the help of soft magnetic CuNi alloys. Shortly after, the experiments provided the evidence of junctions with negative critical current (π -shift of the current-phase relation, CPR) through phase-sensitive experiments [14] and demonstrated temperature induced transition to this π -state [15]. At the same time, other challenges appeared in the field.

One of the main problems of superconductive electronics is the creation of φ -junction, the structure with nontrivial phase φ in the ground state. Implementation of these structures in conventional schemes RSFQ-logic (Rapid Single Flux Quantum) can reduce the size of the circuits and increase their speed [16-18]. Another possibility is development of quantum bits using φ -contacts. It would mean downsizing and decreased sensitivity to external noise [19-22]. However, the development of φ -junction reveals the problem of miniaturization. Most of earlier proposals are addressed to complex structures in the long Josephson junction regime ($W > \lambda_J$) [23-28].

The relation between supercurrent I_S across a heterostructure and its Josephson phase φ plays an important role for various superconducting devices. In standard structures superconductor-insulator-superconductor (SIS) with tunnel type of conductivity, the CPR has the sinusoidal form

$I_s(\varphi) = A \sin(\varphi)$. In SNS or SINIS junctions (N is for normal metal here) with metallic type of conductivity in the weak link area the decrease in the temperature T increases the deviations from the $\sin(\varphi)$ form and $I_s(\varphi)$ achieves its maximum at $\pi/2 \leq \varphi \leq \pi$. In SIS junctions the amplitude B of the second harmonic in CPR, $B \sin(2\varphi)$, is the value of the second order of smallness (with respect to the probability of tunneling through the barrier) and is negligibly small for all T . In sandwiches with normal metal in the vicinity of critical temperature T_c $A \approx \text{Const} \times (T_c - T)$, but the second harmonic amplitude in CPR is also small here. At low temperatures A and B have comparable magnitudes, thus giving rise to qualitative modifications of CPR shape.

Nota bene: in all discussed types of structures the ground state corresponds to phase $\varphi = 0$, since at $\varphi = \pi$ a junction is at nonequilibrium state.

New opportunities open up in Josephson junctions involving ferromagnets as weak link materials. The so-called π -state in SFS Josephson junctions (with π -shift of the CPR) was predicted in 1970s and observed in experiments at the beginning of this century [29-32]. Contrary to SIS or SNS junctions, in SFS devices one can have to have the ground state $\varphi_g = \pi$. It was proven experimentally [33] that such π -junctions can be used as on-chip π -phase batteries for self-biasing in various quantum and classical circuits in order to decouple quantum circuits from environment or to replace conventional inductance and strongly reduce the size of an elementary cell [34].

But for some purposes (e.g. for fast memory cells) on-chip φ -batteries are even more attractive. The so-called φ -junctions with Josephson phase $\varphi_g = \varphi$, ($0 < |\varphi| < \pi$) in the ground zero-current state were predicted by Mints [35] for the case of randomly distributed alternating 0- and π -facets along grain boundaries in high T_c superconductors (e.g. cuprates) with d-wave symmetry of the order parameter. It can be shown that φ -junctions can be realized on the base of 0- and π -segments in an inhomogeneous structure SFS structure [36]. Depending on the weights of the segments the state with an ‘‘average’’ phase φ_g can be generated if the mismatch between the segments is relatively small, $-\pi \leq \varphi_g \leq \pi$. Remarkable progress was recently achieved on implementation of φ -junctions within competing concepts [37-42].

In order to create a φ -junction one need a Josephson structure with non-sinusoidal CPR. In the simplest case, this CPR is written as follows

$$I_s(\varphi) = A \sin(\varphi) + B \sin(2\varphi), \quad (1.1)$$

where the following amplitudes of the CPR harmonics, A , and, B , are needed

$$|B| > |A|/2, B < 0. \quad (1.2)$$

In SIS and SFS structures, the requirements (1.2) can not be met. In SFS junctions in the vicinity of 0 to π transition the amplitude of the first harmonic in CPR is close to zero, thus opening an opportunity for creating a φ - battery, if B is negative. But in both the SFS and the SIFS structures with high transparencies of SF interfaces decay length for superconducting correlations induced into F-layer is complex: $\xi_H = \xi_1 + i\xi_2$. Here $A \approx \exp\{-L/\xi_1\} \cos(L/\xi_2)$, $B \approx -\exp\{-2L/\xi_1\} \cos(2L/\xi_2)$, and for $L = (\pi/2)\xi_2$ corresponding to the first $0 - \pi$ transition the second harmonic amplitude B is always positive.

The way forward is possible here due to the idea of the so-called “current in plane” SFS devices [44, 45] with NF or FNF multilayers in the weak link region consisting and with the supercurrent flowing parallel to FN interfaces. In these structures, superconductivity is induced from the S electrodes into the normal (N) film, while F films serves as a source of spin polarized electrons and provides an effective control for exchange field. The reduction of effective exchange energy here permits to increase the decay length from the scale of the order of 1 nm up to 100 nm. But the approaches developed during the analysis of such structures can not help us: the calculations performed did not go beyond linear approximation, hence the amplitude of the second harmonic in the CPR is considered small.

The purpose of this chapter is to demonstrate that the mentioned concept of the current-in-plane devices (see Fig. 1) can be used as effective φ -shifters. The structure of the paper is the following. In Sec. 2 we formulate quantitative model in terms of Usadel equations with Kupriyanov-Lukichev boundary conditions. In Sec 3 the criteria of zero-current φ -state existence are derived for different types of S-FN-S structure. Finally in Sec.4 we consider properties of real materials and estimate the possibility to realize φ -junctions using up-to-date technology.

2. MODEL

We consider here different types of symmetric multilayered structures (see sketches on Fig.1). The structures consist of superconducting electrodes contacting either the end-wall of a FN bilayer (ramp type structures) or the surface of F or N films (overlap type geometry with thickness d_F , d_N respectively). The conditions of a dirty limit are fulfilled for all metals; effective electron-phonon coupling constant is zero in F and N films. We assume that the parameters γ_{BN} and γ_{BF} for the transparencies of NS and FS interfaces are large enough

$$\gamma_{BN} = \frac{R_{BN} \mathcal{A}_{BN}}{\rho_N \xi_N} \gg \frac{\rho_S \xi_S}{\rho_N \xi_N},$$

$$\gamma_{BF} = \frac{R_{BF} \mathcal{A}_{BF}}{\rho_F \xi_F} \gg \frac{\rho_S \xi_S}{\rho_F \xi_F},$$
(1.3)

in order to neglect suppression of superconductivity in S banks. Here R_{BN}, R_{BF} and $\mathcal{A}_{BN}, \mathcal{A}_{BF}$ are the resistances and areas of the SN and SF interfaces, ξ_S, ξ_N and ξ_F ; ρ_S, ρ_N and ρ_F are the decay lengths and resistivities for the corresponding materials.

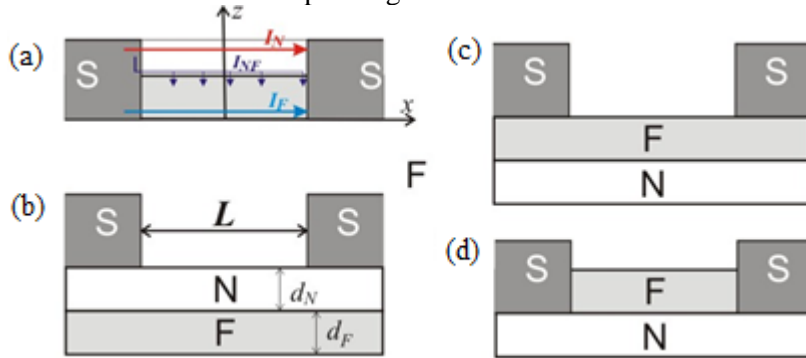


Figure 1. (a) The S – NF – S junction, (b) the SNF – NF – FNS junction, (c) the SFN – FN – NFS junction and (d) the SN – FN – NS junction.

Under the above conditions the problem of calculation of the supercurrent in the structures reduces to solution of the set of Usadel equations [47]

$$\frac{\xi^2}{G_\omega} \partial \left[G_\omega^2 \partial \Phi_\omega \right] - \frac{\tilde{\omega}}{\pi T_C} \Phi_\omega = 0, G_\omega = \frac{\tilde{\omega}}{\sqrt{\tilde{\omega}^2 + \Phi_\omega \Phi_{-\omega}^*}},$$
(1.4)

where Φ_ω and G_ω are Usadel Green's functions in Φ parametrization. They are $\Phi_{\omega,N}$ and $G_{\omega,N}$ or $\Phi_{\omega,F}$ and $G_{\omega,F}$ in N and F films

correspondingly, $\omega = \pi T(2m+1)$ are Matsubara frequencies ($m=0,1,2,\dots$). Here we use $\tilde{\omega} = \omega + iH$, and H is the exchange field in ferromagnetic material, $\xi^2 = \xi_{N,F}^2 = D_{N,F} / 2\pi T_C$ for N and F layers respectively, $D_{N,F}$ are diffusion coefficients, $\partial = (\partial/\partial x, \partial/\partial z)$ is 2D gradient operator. To write equations (1.4), we have chosen the z and x axis in the directions, respectively, perpendicular and parallel to the plane of N film. We always set the origin in the middle of the junction at the free interface of F-film (see Fig.1).

We calculate the supercurrent $I_S(\varphi)$ by integrating the standard expressions for the current density $j_{N,F}(\varphi, z)$ over the junction cross-section:

$$\frac{2ej_{N,F}(\varphi, z)}{\pi T} = \sum_{\omega=-\infty}^{\infty} \frac{iG_{\omega}^2}{\rho_{N,F}\tilde{\omega}_{N,F}^2} \left[\Phi_{\omega} \frac{\partial \Phi_{-\omega}^*}{\partial x} - \Phi_{-\omega}^* \frac{\partial \Phi_{\omega}}{\partial x} \right], \quad (1.5)$$

$$I_S(\varphi) = W \int_0^{d_F} j_F(\varphi, z) dz + W \int_{d_F}^{d_F+d_N} j_N(\varphi, z) W dz,$$

where W is the width of the structures, which is supposed to be small compared to Josephson penetration depth. It is convenient to perform the integration in (1.5) in F and N layers separately along the line located at $x=0$; z -component of supercurrent vanishes from considerations of symmetry.

Eq.(1.5) must be supplemented by the boundary conditions. Since these conditions link the Usadel Green's functions corresponding to the same Matsubara frequency ω , we may simplify the notations by omitting the subscript ω . At the NF interface the boundary conditions have the form:

$$\gamma_{BFN} \xi_F \frac{\partial \Phi_F}{\partial z} = -\frac{G_N}{G_F} \left(\Phi_F - \frac{\tilde{\omega}}{\omega} \Phi_N \right), \quad (1.6)$$

$$\gamma_{BNF} \xi_N \frac{\partial \Phi_N}{\partial z} = \frac{G_F}{G_N} \left(\Phi_N - \frac{\omega}{\tilde{\omega}} \Phi_F \right),$$

$$\gamma_{BFN} = \frac{R_{BFN} \mathcal{A}_{BFN}}{\rho_F \xi_F} = \gamma_{BNF} \frac{\rho_F \xi_F}{\rho_N \xi_N},$$

where R_{BFN} and \mathcal{A}_{BFN} are the resistance and area of the NF interface.

The conditions at free interfaces are

$$\frac{\partial \Phi_N}{\partial n} = 0, \quad \frac{\partial \Phi_F}{\partial n} = 0. \quad (1.7)$$

The partial derivatives in (1.7) are taken in the direction, which is normal to the boundary, so that n can be either z or x depending on the particular geometry of the junction.

We have ignored the suppression of superconductivity in S-banks, and hence we have:

$$\Phi_S(\pm L/2) = \Delta \exp(\pm i\varphi/2), \quad G_S = \frac{\omega}{\sqrt{\omega^2 + \Delta^2}}, \quad (1.8)$$

where Δ is magnitude of the order parameter here. Therefore for NS and FS interfaces we have:

$$\begin{aligned} \gamma_{BN} \xi_N \frac{\partial \Phi_N}{\partial n} &= \frac{G_S}{G_N} (\Phi_N - \Phi_S(\pm L/2)), \\ \gamma_{BF} \xi_F \frac{\partial \Phi_F}{\partial n} &= \frac{G_S}{G_F} \left(\Phi_F - \frac{\tilde{\omega}}{\omega} \Phi_S(\pm L/2) \right). \end{aligned} \quad (1.9a)(1.9b)$$

As in Eq. (1.7), n in Eqs. (1.9a), (1.9b) is a normal vector directed into material mentioned in derivative.

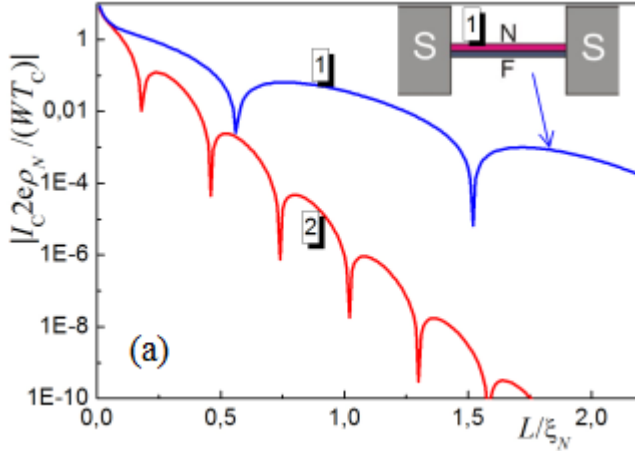
For the structure presented at Fig.1a, the boundary-value problem (1.4) - (1.9b) was solved analytically in the linear approximation [45], when

$$G_N \equiv \text{sgn}(\omega), \quad G_F \equiv \text{sgn}(\omega). \quad (1.10)$$

In the following sections we will go beyond the linear approximation in order to find new properties of CPR of the structures under consideration.

3. RAMP- AND OVERLAP-TYPE GEOMETRIES

The ramp type Josephson consists of the NF bilayer, laterally connected with S-banks (see Fig.1a and insets at Fig. 2).



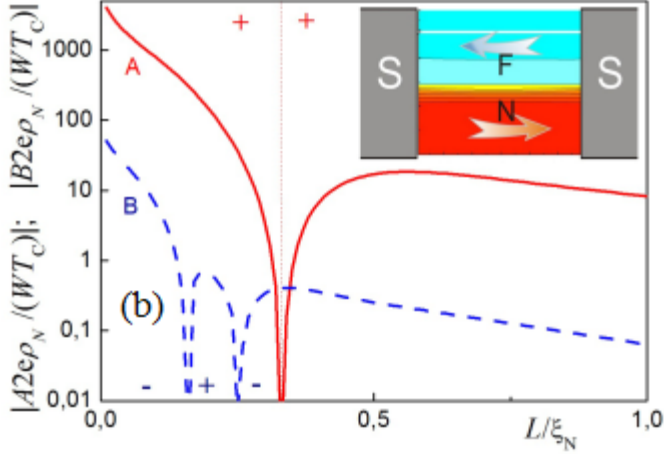


Figure 2. (a) Normalized critical current I_C versus normalized spacing L between S- electrodes for SFS structure (2) and for heterostructures with thin NF bilayer (1). (b) CPR harmonic amplitudes A (solid line) and B (dashed line) for S-NF-S structure versus spacing L for heterostructures with thick NF bilayer. Inset presents current distribution calculated for for the case of φ -junction existence ($L = 0.33\xi_N$). The colors in the inset correspond to the intensity and sign of the current density concentration in the horizontal (x) direction.

Properties of the considered structure are significantly different in the two opposite limits: in the limits of thin (1) / thick (2) N- and F- films. In the first case (thin films) the properties resemble the properties of the SFS junction with slightly enlarged coherence length (see Fig.2a). For the second case (thick films) the weak link region may be divided into domains with the supercurrent flowing in the opposite directions. The current density map along S-NF-S two-dimensional junction is shown in the inset at Fig.2b. Hence the first harmonic amplitudes in the CPR, A , may be equal to zero due to cancellation of the current contributions from F- and N- channels in π - and in 0-state, respectively. For certain parameters of NF bilayer (mainly for d_N , d_F) one can obtain stable φ -state due to the strongly nonsinusoidal CPR with negative amplitude of the second harmonic, B .

In general case, there are three characteristic scales for the decay of superconducting correlations: ξ_N , $\xi_H = \xi_1 + i\xi_2$, $\zeta = \zeta_1 + i\zeta_2$ [48]. The first two scales determine decay and oscillations of superconducting correlations far from FN interface, while the last one, ζ , describes their behavior in its vicinity. Similar length scale ζ occurs near a domain wall in ferromagnets [49]. Here the exchange field is averaged out for antiparallel directions of magnetizations, and the decay length of superconducting correlations tends to ξ_N . At FN interface, the flow of spin-polarized electrons from F to N metal and reverse flow of unpolarized electrons from N to F suppresses the exchange field thus providing the existence of ζ .

Under certain set of parameters these scales, ζ_1 , and, ζ_2 , can be comparable with ξ_N , which is typically much larger than ξ_1 and ξ_2 ($\xi_F \sqrt{\pi T_C / H}$ for $H \gg \pi T_C$).

The existence of three decay scales, ξ_N , ζ , and ξ_H , should lead to appearance of three contributions to total supercurrent, I_N , I_{FN} and I_F , respectively. The main contribution to “normal” component I_N comes from the supercurrent, which is uniformly distributed in the N-film. In accordance with the mentioned above qualitative analysis [50], it is the only current component which leads to a negative value of the amplitude of the second harmonic B in the CPR. The smaller is the distance between the S-electrodes, L , the larger is this contribution to the total supercurrent. To create a φ -contact, one need to compensate the amplitude of the first harmonic, A , in a total current to a value that satisfies the conditions (1.2). Contribution to this amplitude A from I_N also increases with decreasing spacing L . Obviously, it's difficult to suppress the coefficient A due to the “boundary” contribution I_{FN} only, since I_{FN} flows through thin near-boundary layer. Therefore, strong reduction of A can be obtained as a result of competition between I_N and I_F currents flowing in opposite directions in N and F films far from FN interface. Note that the oscillatory behaviour of the $I_F(L)$ dependence allows to met conditions (1.2) in a certain range of L . The role of “boundary” contribution I_{FN} in the required balance between I_N and I_F can be understood by solving the boundary value problem (1.4) - (1.9b) which admits an analytic solution in some interesting cases.

Spacing L is small. Solution of the boundary-value problem (1.4)-(1.9b) can be simplified in the limit of small distance between superconducting electrodes:

$$L \ll \min \{ \xi_1, \xi_N \}. \quad (1.11)$$

In this case we decide to neglect non-gradient terms in (1.4). Hence the contributions to the total current resulting from the redistribution of currents near the FN interface cancel each other leading to $I_{FN} = 0$ [50]. As a result, the total current $I_S(\varphi)$ is a sum of the following two terms

$$I_S(\varphi) = I_N(\varphi) + I_F(\varphi),$$

$$\frac{2eI_N(\varphi)}{\pi TWd_N} = \frac{1}{\gamma_{BN}\xi_N\rho_N} \sum_{\omega=-\infty}^{\infty} \frac{\Delta^2 G_N G_S \sin(\varphi)}{\omega^2} \quad (1.12)$$

$$\frac{2eI_F(\varphi)}{\pi TWd_F} = \frac{1}{\gamma_{BF}\xi_F\rho_F} \sum_{\omega=-\infty}^{\infty} \frac{\Delta^2 G_N G_S \sin(\varphi)}{\omega^2} \quad (1.13)$$

where $G_N = \frac{\omega}{\sqrt{\omega^2 + \Delta^2 \cos^2\left(\frac{\varphi}{2}\right)}}$. The “normal” and “ferromagnet”

currents $I_N(\varphi)$ and $I_F(\varphi)$ flow independently across the corresponding parts of the weak link. The $I_{N,F}(\varphi)$ dependencies coincide with those calculated previously for double-barrier junctions [51] when value L lies within the interval from the inequalities (1.11).

It follows from (1.12), (1.13) that in this case the amplitude of the first harmonic for “ferromagnet” component $I_F(\varphi)$ is always positive and the condition (1.2) can not be met.

Spacing L is intermediate. In this limit we have

$$\xi_1 = L = \xi_N \quad (1.14)$$

and for the values of suppression parameters at SN and SF interfaces satisfying the conditions (1.3), the boundary problem (1.4)-(1.9b) can be solved analytically for sufficiently large magnitude of suppression parameter γ_{BFN} . It was shown in [50] that under these restrictions in the first approximation we can neglect the suppression of superconductivity in the N film due to proximity with the F layer:

$$\Phi_N = \Delta \cos\left(\frac{\varphi}{2}\right) + i \frac{\Delta G_S \sin\left(\frac{\varphi}{2}\right)}{\gamma_{BN} G_N} \frac{x}{\xi_N}, \quad G_N = \frac{\omega}{\sqrt{\omega^2 + \Delta^2 \cos^2\left(\frac{\varphi}{2}\right)}}, \quad (1.15)$$

while spatial distribution of $\Phi_F(x, z)$ includes three terms.

The first two terms in (1.15) describe the influence of the N film, while the last one has the form well known for SFS junctions. Expression (1.5) allows us to represent the total supercurrent in the form:

$$I_S(\varphi) = I_N(\varphi) + I_F(\varphi) + I_{FN}(\varphi). \quad (1.16)$$

Here $I_N(\varphi)$ is given by the expression (1.12). The second term in (1.16) in the limit of small transparencies of SF interfaces is as follows:

$$\frac{2eI_F(\varphi)}{\pi T W d_F} = \frac{\Delta^2 \sin(\varphi)}{\gamma_{BF}^2 \xi_F \rho_F} \sum_{\omega=-\infty}^{\infty} \frac{G_S^2}{\omega^2 \sqrt{\tilde{\Omega}} \sinh(2q_L)}, \quad (1.17)$$

where $q_L = L\sqrt{\tilde{\Omega}}/2\xi_F$, $\tilde{\Omega} = |\Omega| + iH\text{sgn}(\Omega)/\pi T_C$, $\Omega = \omega/\pi T_C$.

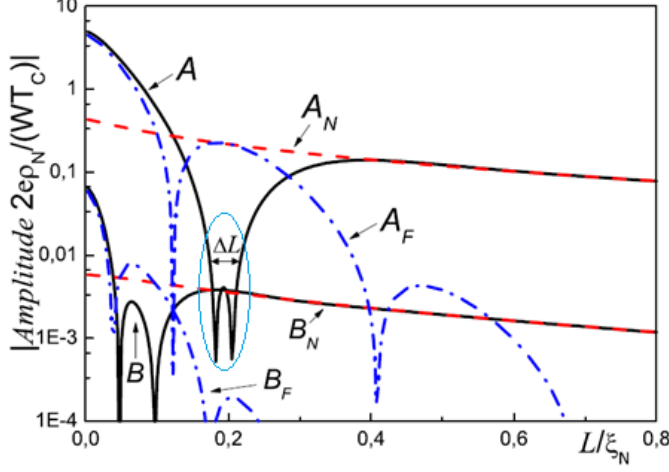


Figure 3. Numerical results for the amplitudes A, B in the CPR of the ramp-type S-NF-S structure ($d_N = 0.1\xi_N$; $d_F = 1.06\xi_N$) and their components A_N, A_F, B_N, B_F vs spacing L at $T = 0.7T_C$. Parameters are chosen to form enhanced φ -state interval marked by “ ΔL ”.

The last contribution contains three components

$$I_{FN}(\varphi) = I_{FN1}(\varphi) + I_{FN2}(\varphi) + I_{FN3}(\varphi). \quad (1.18)$$

with additional smallness parameters γ_{BFN}^{-1} and $\gamma_{BFN}^{-1}\xi_F/\xi_N$ in comparison with the “ferromagnet” component $I_F(\varphi)$. Nevertheless, these terms should be taken into account in the analysis because they decay significantly slower than $I_F(\varphi)$ with increasing spacing L .

Stable zero-current φ -state. Here we need relative large absolute value for the amplitude of the second harmonic (and hence we need low temperatures). But in the limit $T = T_C$ we can go from summation to integration over ω in (1.12), (1.17). Thus

$$\frac{2eI_N(\varphi)}{Wd_N} = \frac{\Delta}{\gamma_{BN}\xi_N\rho_N} K\left(\sin\frac{\varphi}{2}\right)\sin(\varphi), \quad (1.19)$$

where $K(x)$ is the complete elliptic integral of the first kind. We expanded the obtained expression (1.19) in the Fourier series:

$$A_N = Q_0 \frac{8}{\pi} \int_0^1 x^2 \sqrt{1-x^2} K(x) dx = Y_A Q_0, \quad (1.20)$$

$$B_N = 2A_N - \frac{32}{\pi} Q_0 \int_0^1 x^4 \sqrt{1-x^2} K(x) dx = Y_B Q_0, \quad (1.21)$$

where $Q_0 = \Delta W d_N / e \gamma_{BN} \xi_N \rho_N$. A_N, B_N are the first and the second harmonic amplitudes of $I_N(\varphi)$,

$$Y_A = \frac{2\pi^2}{\Gamma^2\left(-\frac{1}{4}\right)\Gamma^2\left(\frac{7}{4}\right)}; 0.973,$$

$$Y_B = 2Y_A - \frac{\pi}{2_3} F_2\left(\frac{1}{2}, \frac{1}{2}, \frac{5}{2}; 1, 4; 1\right); -0.146,$$

where $\Gamma(z)$ is the well-known Gamma-function and ${}_pF_q$ is generalized hypergeometric function.

Evaluation of the sums in (1.17) can be done for $H \gg \pi T_C$ and $T = T_C$ resulting in sinusoidal “ferromagnet” component $I_F(\varphi) = A_F \sin(\varphi)$ with

$$A_F = P_0 \frac{2}{\sqrt{h}} \exp(-\kappa L) \cos\left(\kappa L + \frac{\pi}{4}\right), \quad (1.22)$$

$\kappa = \sqrt{h} / \sqrt{2} \xi_F$, $h = H / \pi T_C$ and $P_0 = \Delta W d_F / e \gamma_{BF}^2 \xi_F \rho_F$. Substitution of (1.20), (1.21) into the inequalities (1.2) gives analytical form of the φ -state conditions for the ramp-type structure:

$$\left| Y_A + \frac{1}{\varepsilon} \Psi(L) \right| < 2 |Y_B|, \quad \varepsilon = \frac{\sqrt{h} \gamma_{BF}^2}{2 \gamma_{BN}} \frac{d_N \xi_F \rho_F}{d_F \xi_N \rho_N}, \quad (1.23)$$

$$\Psi(L) = \exp(-\kappa L) \cos\left(\kappa L + \frac{\pi}{4}\right).$$

These expressions give us the limitation on geometrical and material parameters of the considered junctions providing the existence of stable zero-current φ -state. Function $\Psi(L)$ has the first minimum at $\kappa L = \pi/2$, $\Psi(\pi/2\kappa) \approx -0.147$. For large enough values of ε inequality (1.23) can not be fulfilled at any spacing L . Thus solutions exist only in the area with upper limit

$$\varepsilon < \frac{-\Psi(\pi/2\kappa)}{Y_A - 2|Y_B|} \approx 0.216. \quad (1.24)$$

At $\varepsilon \approx 0.216$ the left hand side of inequality (1.23) equals to its right hand part providing the nucleation of an interval of κL in which we can expect the creation of a φ -structure. This interval increases with decrease of ε and achieves its maximum length

$$1.00 \lesssim \kappa L \lesssim 2.52, \quad (1.25)$$

at $\varepsilon = \frac{-\Psi(\pi/2\kappa)}{Y_A + 2|Y_B|} \approx 0.116$. Nota bene: at $\varepsilon = -\Psi(\pi/2\kappa)/Y_A \approx 0.151$

there is a transformation of the left hand side local minimum in (1.23), which occurs at $\kappa L = \pi/2$, into local maximum; so that at $\varepsilon \approx 0.116$ the both sides of (1.23) become equal to each other, and the interval (1.25) of φ -contact existence subdivides into two parts. With a further decrease of ε these parts are transformed into bands, which are localized in the vicinity of the $0-\pi$ transition point ($A_N + A_F = 0$). These narrow valleys of required parameters take place at $\kappa L = \pi/4$ and $\kappa L = 5\pi/4$. The width of the mentioned bands decreases with decrease of ε .

Thus, our analysis has shown that for

$$0.12 \leq \varepsilon \leq 0.2 \quad (1.26)$$

we can expect the creation of φ -structure in a sufficiently wide range ΔL of spacing between the S-electrodes. One can determine the value ΔL from equation (1.23).

Let us take into account the impact of the interface term $I_{FN}(\varphi)$. In the considered case we have [50] the following contributions:

$$I_{FN1}(\varphi) = \frac{2U_0\xi_F \exp\left(-\frac{\kappa L}{2}\right) \cos\left(\frac{\kappa L}{2} - \frac{\pi}{4}\right)}{\gamma_{BF}\gamma_{BN1}\xi_N h^{3/2}} \sin(\varphi) \quad (1.27)$$

$$I_{FN2}(\varphi) = -\frac{\sqrt{2}U_0\xi_F}{4h^{3/2}\gamma_{BF}\gamma_{BN1}\xi_N} \sin(\varphi) K \sin\left(\frac{\varphi}{2}\right) \quad (1.28)$$

$$I_{FN3}(\varphi) = -\frac{2U_0\xi_F \exp\left(-\frac{\kappa L}{2}\right) \sin\left(\frac{\kappa L}{2}\right)}{h\gamma_{BF}} \sin(\varphi) K \sin\left(\frac{\varphi}{2}\right) \quad (1.29)$$

where $U_0 = \Delta W / e\gamma_{BFN}\rho_F$. In the range of spacings $\pi/4 < \kappa L < 5\pi/4$ the currents $I_{FN2}(\varphi)$ and $I_{FN3}(\varphi)$ are less than zero. These contributions have the same form of CPR as it was for the “normal” $I_N(\varphi)$ term, and due to negative sign suppress the magnitude of supercurrent across the junction thus making the inequality (1.23) easier to perform. The requirement $B < 0$

imposes additional restriction on the value of the suppression parameter γ_{BFN}

$$\gamma_{BFN} > \frac{\rho_N \xi_N}{h d_N \rho_F} \left(\frac{\xi_F}{\xi_N \gamma_{BFN} h^{1/2}} + \frac{\gamma_{BN}}{\gamma_{BF}} \right). \quad (1.30)$$

In order to obtain this inequality we have used the fact that in the range of distances between the electrodes $\pi/4 < \kappa L < 5\pi/4$ depending on κL factor in (1.29) is of the order of unity. It follows from (1.30) that for a fixed value of γ_{BFN} domain of φ -structure existence extends with increase of thickness of N-film d_N . Stable zero-current -state is impossible if d_N becomes smaller than the critical value, d_{NC} ,

$$d_{NC} = \frac{\rho_N \xi_N}{h \rho_F \gamma_{BFN}} \left(\frac{\xi_F}{\xi_N \gamma_{BFN} h^{1/2}} + \frac{\gamma_{BN}}{\gamma_{BF}} \right). \quad (1.31)$$

The existence of the critical thickness d_{NC} follows from the fact that the amplitude B in “normal” component I_N is proportional to d_N , while in I_{FN} term B is independent on d_N . The sign of $I_{FN1}(\varphi)$ term is positive for $\pi/4 < \kappa L < 3\pi/4$ and negative for $3\pi/4 < \kappa L < 5\pi/4$ thus providing an advantage for a φ -structure realization for the spacings which correspond to the second interval.

Figure 4b illustrates our analytical results. The solid line at the figure is the absolute value of the first harmonic amplitude versus spacing L between S-banks. It is the sum of two components, which were calculated from expressions (1.17) (dash-dotted line) and (1.12) (dashed line). The dash-dot-dotted line at Fig. 4b is the amplitude of the second harmonic in “normal” component (1.12). The dotted line is the $I_{FN}(L)$ dependence calculated from (1.18). We made all calculations for the following set of parameters, which is close to those in real experiment: $d_N = 0.1\xi_N$, $d_F = 0.65\xi_N$, $\gamma_{BN} = 0.1$, $\gamma_{BF} = 1$, $\gamma_{BNF} = 10$, $\xi_F = 0.1\xi_N$, $\rho_N = \rho_F$, $T = 0.7T_C$, $H = 10T_C$. All the amplitudes in CPRs were normalized using factor $(2e\rho_N/(WT_C))^{-1}$. There is an interval of spacings L , when the currents in N and F layers flow in opposite directions and the points of $0-\pi$ transitions for both dependencies become closer to each other. In the entire region between these points, the conditions (1.2) are fulfilled. This is exactly the required “ L -interval”, inside which a zero-current stable φ -state can be achieved. The contribution of I_{FN} term into the total supercurrent in accordance with our analysis is really small.

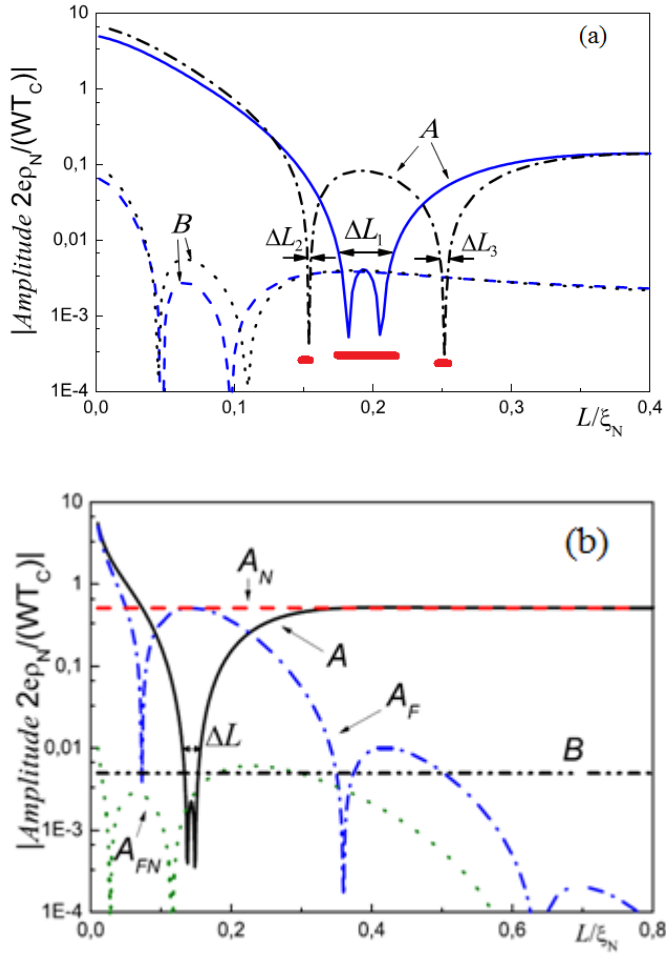


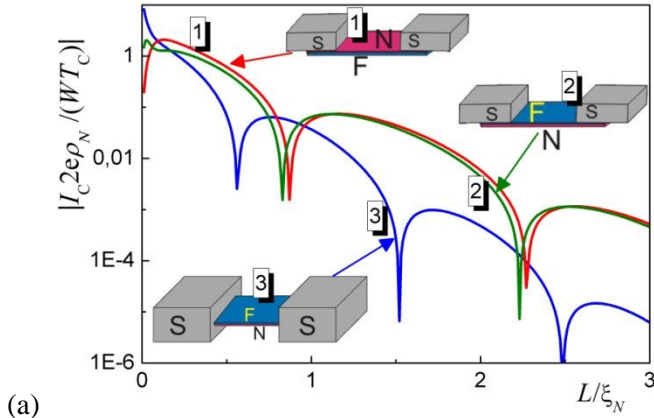
Figure 4. (a) Numerically calculated CPR amplitudes A and B versus electrode spacing L for S-FN-S structures with $d_F = 1.06\xi_N$ (solid and dashed lines respectively). Enhanced φ -interval ΔL_1 is much larger than the sum of “standard” φ -intervals ΔL_2 and ΔL_3 (see dashed lines for $d_F = 1.4\xi_N$). (b) Analytically calculated amplitudes A and B in the CPR of the ramp S-NF-S structure ($d_N = 0.1\xi_N$, $d_F = 0.65\xi_N$) and their components A_N , A_F , A_{FN} versus spacing L at temperature $T = 0.7T_C$. Interval of φ -state existence, ΔL , is marked.

To confirm the obtained findings we have solved the boundary problem (1.4)-(1.9b) for the same set of parameters of the structure except d_F . The results of calculations for two values of F-layer thickness ($d_F = 1.06\xi_N$ and $d_F = 1.4\xi_N$) are presented at Fig.3 and Fig.4a. The solid lines in Fig.3 correspond to the absolute values of the amplitudes of the first,

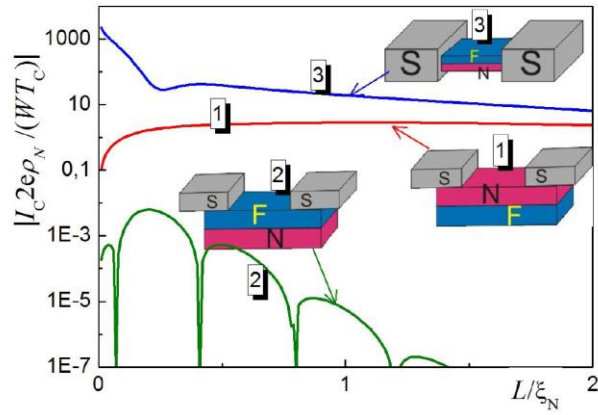
A , and the second, B , harmonic in CPR. The dashed and dash-dotted curves demonstrate the contributions to these amplitudes from the supercurrents, respectively, in N and F layers. The main difference between analytical solutions presented in Fig.4b and the results of numerical calculations belong to the limit of small spacings L . The amplitudes of the first and the second harmonics of the supercurrent in the normal layer decrease with increasing spacing. The points of $0-\pi$ transition of the first harmonic amplitude of the supercurrent in the ferromagnetic are shifted to the right, toward larger distances between superconducting electrodes. The amplitude of the second harmonic here, B_F , in the vicinity of $L \approx 0.2\xi_N$ is negligibly small in comparison with the magnitude of B_N . As a result, the shapes of $A(L)$ curves in Fig. 4b and Fig.3 are nearly the same, with a little bit larger interval of stable zero-current φ -state for the curve representing numerical results.

In Figure 4a we demonstrate the same dependencies $A(L)$ and $B(L)$ as in Fig.3 (solid and dashed lines) together with similar curves calculated for the case $d_F = 1.4\xi_N$ (dash-dotted and dotted lines for A and B). For larger values of d_F we get out of the interval (1.26) and instead of relatively large zone ΔL_1 have to deal with two very narrow intervals ΔL_2 and ΔL_3 located in the vicinity of $0-\pi$ transitions of the first harmonic amplitude A .

Overlap type geometry. From technological point of view the overlap-type geometry (with the overlap length much larger ξ_N , see Fig. 1b) looks more reliable than the ramp-type one. We have shown in our numerical calculations that in the case of thin layers and large transparency of FN interface it doesn't matter, whether the film of normal metal lays above or behind the F-layer (see Fig 5a).



(a)



(b)

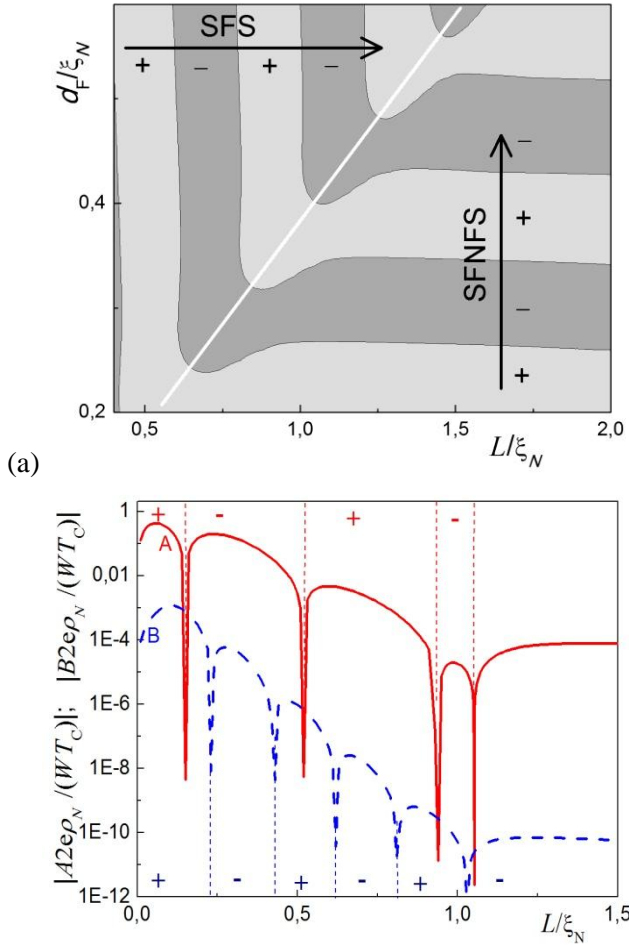
Figure 5. Numerically calculated normalized critical current I_C vs spacing L for (1) SNF-NF-FNS, (2) SFN-FN-NFS and (3) the ramp-type S-NF-S junctions in the case of (a) thin, $d_N = d_F = 0,01\xi_N$, and (b) thick, $d_N = d_F = 3\xi_N$, layers.

At arbitrary layer thickness in SFN-FN-NFS junctions (Fig. 5b) the large difference between values ξ_N and ξ_F results in formation of two (SFS and SFNFS) competing parallel current channels. In SNF-NF-FNS structures the current through long SNFNS channel is always much smaller than the current through SNS pathway. In SFN-FN-NFS structures the signs of the critical current I_C and harmonic amplitudes in the SFS channel are controlled by the distance L between S-banks. The sign of the SFNFS contribution to the total supercurrent is a function of ferromagnetic layer thickness, d_F . In Fig. 6a we represent the phase diagram of the CPR harmonic amplitudes in (L, d_F) plane: the proper choice of the F-film topology allows

(1) to suppress the amplitude of the first harmonic in CPR

(2) to make the necessary sign for zero-current φ -state existence for the amplitude B of the second one (see Fig. 6b).

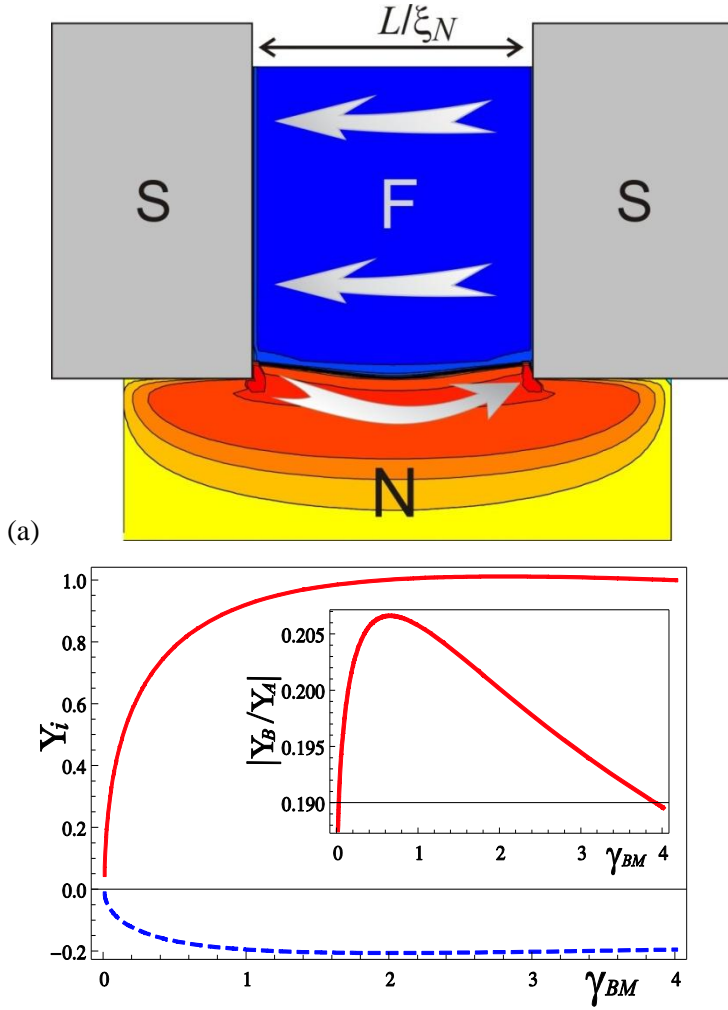
Combined ramp-type-overlap (RTO) junctions. It will be somewhat



(b)

Figure 6. (a) (L, dF) phase diagram in SFN-FN-NFS structure with alternating 0- and π -state areas.. (b) Harmonic amplitudes A (solid) and B (dashed line) in the CPR for SFN-FN-NFS structure versus spacing L for heterostructures with thick FN bilayer.

easier to fulfill the conditions for the φ -structure existence due to slight modifications of junction topology. We need here a combination of the ramp-type and the overlap-type configurations, as it is shown in Fig.1. Fig. 7a demonstrates numerical calculations of spatial distribution of supercurrent in RTO φ -structure at Josephson phase $\varphi = \pi / 2$.



(b)

Figure 7. (a) Current distribution along the RTO-type SN-FN-NS structure at $L=0,63\xi_N$, $d_N=\xi_N$, $d_F=2\xi_N$ and $T=0,7T_C$. The intensity of color corresponds to the supercurrent density in directions indicated by arrows. (b) The amplitudes of the first harmonic Y_A (solid line) and the second one Y_B (dashed line) normalized on $2W\Delta/e\rho N_{BN}$ versus reduced thickness γ_{BM} . Inset shows the ratio of harmonics $|Y_B/Y_A|$ versus γ_{BM} .

The supercurrent density is represented through the color saturation . The amplitude of the first harmonic is relatively small here due to opposite current directions in N and F layers. The main feature of the ramp-type-overlap geometry is seen to be specific current distribution in the normal metall layer leading to another

CPR shape with dependence on thickness d_N . Further, the current I_N should saturate as a function of d_N , since normal film regions located at distances larger than ξ_N from SN interface are practically excluded from the process of supercurrent transfer due to exponential decay of proximity-induced superconducting correlations. The RTO structure was analysed in the most interesting practical case of thin layer of normal metall

$$d_N = \xi_N \quad (1.32)$$

$$L = \xi_N, \quad (1.33)$$

and sufficiently large characteristic of boundary transparency γ_{BFN} providing negligibly small suppression of superconductivity in N film due to proximity with F layer. Under these conditions we can at the first stage consider the Josephson effect in overlap SN-N-NS structure. Then, at the second stage we will use the obtained solutions to calculate supercurrent flowing across the ferromagnetic pathway in the RTO structure [50]. Once again we represent the supercurrent in the following form:

$$I_S(\varphi) = I_N(\varphi) + I_F(\varphi) + I_{FN}(\varphi). \quad (1.34)$$

Expression for the I_N component has the form

$$\frac{2eI_N(\varphi)}{\pi T W d_N} = \frac{2}{\rho_N \xi_N \sqrt{\gamma_{BM}}} \sum_{\omega=-\infty}^{\infty} \frac{r^2 \delta^2 \sin \varphi \sqrt{(\Omega \gamma_{BM} + G_S)}}{\sqrt{2\Omega \mu^2 (\sqrt{\Omega^2 + r^2 \delta^2} + \mu)}}, \quad (1.35)$$

where $r = G_S / (\Omega \gamma_{BM} + G_S)$, $\gamma_{BM} = \gamma_{BN} d_N / \xi_N$ and $\mu = \sqrt{\Omega^2 + r^2 \delta^2 \cos^2(\varphi/2)}$, $\delta = \Delta / \pi T_C$.

The ‘‘ferromagnetic’’ term $I_F(\varphi)$ in (1.34) is the supercurrent through one dimensional double barrier SFS structure defined by Eq. (1.17), while the FN-interface term $I_{FN}(\varphi)$ was discussed before.

The larger is the relative amplitude of the second harmonic (or the lower is the temperature of a junction compare to T_C), the better we meet the conditions for the implementation of a zero-current φ -state. At high temperature $T = T_C$ we can transform summation into integration over ω in (1.35) and calculate numerically the dependences A and B :

$$A_N = \frac{2W\Delta}{e\rho_N \gamma_{BN}} Y_A, \quad (1.36)$$

$$B_N = \frac{2W\Delta}{e\rho_N \gamma_{BN}} Y_B \quad (1.37)$$

on suppression parameter γ_{BM} . The results of our calculations $Y_A(\gamma_{BM})$ and $|Y_B|(\gamma_{BM})$ are presented in Fig. 7b. Both Y_A and $|Y_B|$ increase with increasing of γ_{BM} and saturate at $\gamma_{BM} \approx 1$. Inset in Fig. 7b shows the ratio of the harmonics $|Y_B/Y_A|$ as a function of γ_{BM} . It achieves maximum at $\gamma_{BM} \approx 0.64$, thus it determines the optimal values of normalized amplitudes of the first $Y_A \approx 0.844$ and the second $Y_B \approx -0.175$ harmonics of the current in the film of normal metal. It is seen from the inset in Fig. 7b, that the ratio $|Y_B/Y_A|$ is slowly decreasing function of γ_{BM} . Therefore, the estimates given below for $\gamma_{BM} = 0.64$ are applicable in a wide range of parameters: $0.5 \leq \gamma_{BM} \leq 10$.

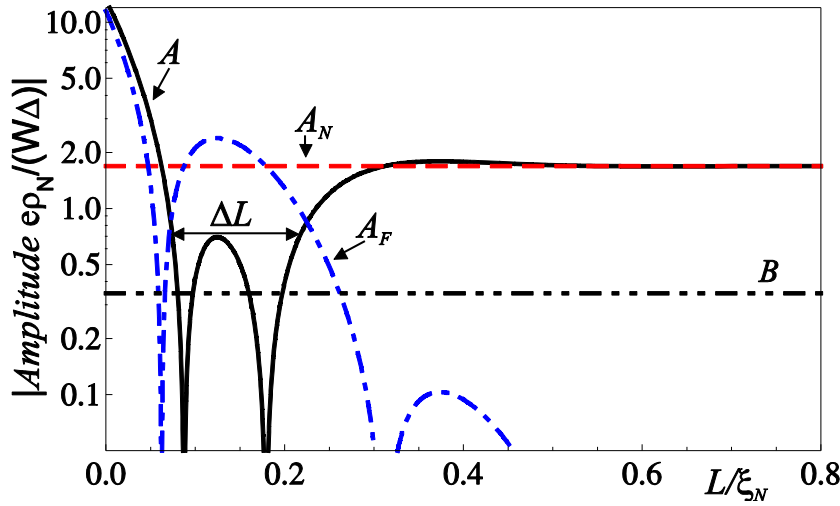


Figure 8. The amplitudes A , A_N , A_F , B of the CPR harmonics vs spacing L for the RTO junction at small temperature $T \ll T_C$, $\gamma_{BM} = 0.64$ and $\varepsilon = 0.123$. The mark " ΔL " shows enhanced φ -state interval.

Hence we can write down the condition of zero-current φ -state existence similar to (1.23)

$$\left| Y_A + \frac{1}{\varepsilon} \Psi(L) \right| \leq 2|Y_B|, \varepsilon = \frac{\sqrt{\hbar} \gamma_{BF}^2 \xi_F \rho_F}{\gamma_{BN} d_F \rho_N}, \quad (1.38)$$

$$\Psi(L) = \exp(-\kappa L) \cos\left(\kappa L + \frac{\pi}{4}\right),$$

with modified dimensionless parameter ε . The wide region of φ -state existence still can be found if ε is within the interval

$$0.123 \leq \varepsilon \leq 0.298. \quad (1.39)$$

κL value here satisfies the condition (1.38). As follows from (1.38), interval of κL product gains its maximum length

$$0.94 \leq \kappa L \leq 2.72, \quad (1.40)$$

at $\varepsilon = 0.123$. These intervals are slightly larger than those given by (1.25) for the ramp-type junction topology.

Fig. 8 represents our main results for the interval of φ -state existence, ΔL , in the ideal case of $T = T_C$, $\gamma_{BM} = 0.64$ and $\varepsilon = 0.123$. The corresponding set of parameters $d_N = 0.64\xi_N$, $d_F = 1.45\xi_N$, $\gamma_{BN} = 1$, $\gamma_{BF} = 1$, $\xi_F = 0.1\xi_N$, $\rho_N = \rho_F$, $H = 10T_C$ was substituted in Eqs. (1.17), (1.35). The solid line is an absolute value of the first harmonic amplitude; its normal, A_N , and ferromagnetic, A_F , components are shown by dashed and dash-dotted lines respectively. The second harmonic amplitude is shown as dash-dot-dotted curve. It's clear that $|A|$ is small enough in the wide region ΔL and reaches the value of $|2B|$ only at local maximum. The increased width of ΔL is provided by geometric attributes of RTO type structure.

Let us illustrate the range of nontrivial ground phase φ_g with the help of Fig. 9. Here the total supercurrent I_S is shown as a function of Josephson phase φ and spacing L . It means that each L -section of this 3D graph is a single CPR. Thick red lines mark the ground state phases at each value of L . In the range of small and large spacing L ground phase is located at $\varphi_g = 0$. However, in the ΔL -interval the CPRs become significantly nonsinusoidal and demands ground phase φ_g to split and go to π from both sides; then π -state is realized at $\kappa L = \pi/2$. Clearly, for $\varepsilon \geq 0.123$ the value $\varphi_g = \pi$ can not be reached (see Fig. 9a), while in the case of $\varepsilon \leq 0.123$ the prolonged π -state region is formed (see Fig. 9c).

4. DISCUSSION AND CONCLUSION

We have shown that zero-current stable φ -state

- can not be achieved in conventional SIS, SNS and SFS structures;
- can be realized in S-NF-S structures with longitudinally oriented NF-bilayers. We have discussed the conditions for creation of φ -junctions in the ramp-type S-NF-S, in the overlap-type SFN-FN-NFS, and in the combined

RTO-type SN-FN-NS geometries. The most favorable suggestions for experimental realization of φ -structure are based on using copper as a normal film ($\xi_N \approx 100 \text{ nm}$ and $\rho = 5 \cdot 10^{-8} \text{ } \Omega\text{m}$) and strongly diluted ferromagnet like FePd or CuNi alloy ($\xi_F \approx 10 \text{ nm}, H \approx 10T_C$) as the F-layer. We would like to chose Nb ($T_C \approx 9K$) as a material for S-electrodes since it is widely used in superconducting applications. We also propose to use sufficiently thick normal layer (above the saturation threshold) when N-layer thickness have almost no effect. After substitution of relevant values into Eqs. (1.39) and (1.40) we came to a fairly broad geometrical margins, within which there is a possibility for creation of φ -structures

$$\begin{aligned} d_N &\geq 50 \text{ nm}, \\ 60 \text{ nm} &\leq d_F \leq 150 \text{ nm}, \\ 7 \text{ nm} &\leq L \leq 22 \text{ nm}. \end{aligned} \quad (1.41)$$

Finally, the width: the last out-of-plane characteristic geometrical scale can be put equal to $W = 140 \text{ nm}$. This allows to maximize “available” supercurrent and conserves the scale of structure in a range of 100 nm . The magnitude of the critical current in the φ -state is determined by the second harmonic amplitude B

$$I_C \sim B_N = \frac{2W\Delta}{e\rho_N\gamma_{BN}} Y_B \approx 1\text{mA}. \quad (1.42)$$

The spreads of geometric scales for creation of φ -junction as well as the magnitude of it's critical current are large enough for practical realization of the considered compact structure.

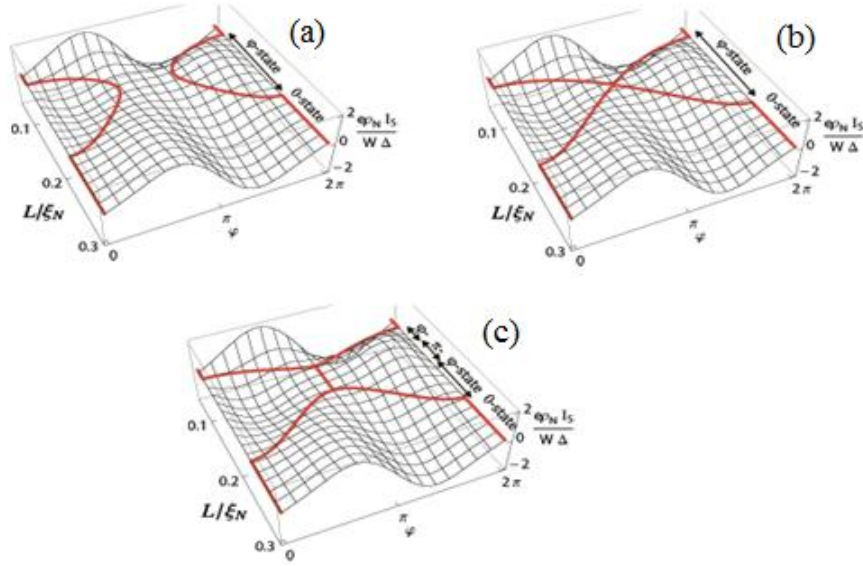


Figure 9. The total supercurrent I_S versus Josephson phase φ and spacing L for the optimal RTO structure at $T \ll T_C$; $Y_{BM} = 0,64$ and at different F-layer thickness parameters (a) $\varepsilon = 0.137$, (b) $\varepsilon = 0.123$, (c) $\varepsilon = 0.111$. The lines mark the ground states phase φ_g [50].

By creating φ -state in a Josephson junction one can fix certain value of ground phase φ_g . Temperature variation slightly shifts the interval of relevant $0 - \pi$ transition and permits one to tune the desired ground state phase. The prospects for the practical use of such structures are related to the possibility of obtaining bistable logic or memory elements on their basis. The characteristic time for the read and, of particularly importance, the write operation here is determined by the Josephson processes and, as a consequence, in many orders of magnitude less than this value in typical cryogenic magnetic-memory cells. Additional superconducting layer in the region of the weak link will increase here the characteristic voltage and frequency to the values that are close to typical for tunnel junctions [52]. Moreover, for the φ -state of the junction the double-well potential is formed at the degeneracy point without any additional fields and ground state splitting provides necessary condition for quantum bits and quantum detectors. To summarize, Josephson φ -structures can be realized using up-to-date technology as a novel basic element for superconducting electronics.

ACKNOWLEDGEMENTS

S.B., I.S., N.K. and M.K. carried out research on current transport for the structures with complex weak-link region (bi-layer) with support of the RSF grant No. 17-12-01079. This work was also supported in part by the Ministry of Education and Science of the Russian Federation, Grant SC 8168.2016.2 and by RFBR grant 16-29-09515-ofi-m.

REFERENCES

1. S.K. Tolpygo, *Low Temp. Phys.* **42**, 463 (2016).
2. A.A. Golubov, M.Yu. Kupriyanov, and E. Il'ichev, *Rev. Mod. Phys.* **76**, 411 (2004).
3. A.I. Buzdin, M.Yu. Kupriyanov, *Pis'ma Zh. Exp. Teor. Fiz.* **52**, 1089 (1990)[*JETP Lett.* **52**, 487 (1990)].
4. L.R. Tagirov, *Physica C* **307**, 145 (1998).
5. T. Kontos, M. Aprili, J. Lesueur, X. Grison. *Phys. Rev. Lett.* **86**, 2, 304 (2001).
6. C. Bell, R. Loloee, G. Burnell, and M. G. Blamire, *Phys. Rev. B* **71**, 180501 (R) (2005).
7. M. Weides, M. Kemmler, E. Goldobin, H. Kohlstedt, R. Waser, D. Koelle, R. Kleiner, *Phys. Rev. Lett.*, **97**, 247001 (2006).
8. A. V. Ustinov, V. K. Kaplunenko, *J. Appl. Phys.* **94**, 5405 (2003).
9. Ya. M. Blanter and F. W. J. Hekking, *Phys. Rev. B* **69**, 024525 (2004).
10. I. B. Sperstad, J. Linder and A. Sodbo, *Phys. Rev. B* **78**, 104509 (2008).
11. M.G. Blamire, J.W.A. Robinson, *Journal of Physics Condensed Matter* **26**, 453201 (2014).
12. M. Eschrig, *Reports on Progress in Physics* **78**, 104501 (2015).
13. V. V. Ryazanov, V. A. Oboznov, A. V. Veretennikov, A. Yu. Rusanov, *Phys. Rev. B* **65**, 02051(R) (2001).
14. S. M. Frolov, D. J. Van Harlingen, V. A. Oboznov, V. V. Bolginov, V. V. Ryazanov, *Phys. Rev. B* **70**, 144505 (2004).
15. V. V. Ryazanov, V. A. Oboznov, A. Yu. Rusanov, A.V. Veretennikov, A.A. Golubov, J. Aarts, *Phys. Rev. Lett.* **86**, 11, 2427 (2001).
16. P. Bunyk, K. Likharev, and D. Zinoviev, *Int. Journal of High Speed Electronics and Systems*, **11**, 1, 257, (2001).
17. T. Ortlev, Ariando, O. Mielke, C. J. M. Verwijs, K. F. K. Foo, H. Rogalla, F. H. Uhlmann, and H. Hilgenkamp, *Science* **312**, 1495 (2006).
18. O. Wetzstein, T. Ortlev, R. Stolz, J. Kunert, H.-G. Meyer, H. Toepfer, *IEEE Trans. on Appl. Supercon.* **21**, 814, (2011).
19. M. H. S. Amin, A. Yu. Smirnov, A. M. Zagoskin, T. Lindstrom, S. A. Charlebois, T. Claeson, A. Ya. Tzalenchuk, *Phys. Rev. B* **73**, 064516-1-5, (2005).
20. N. V. Klenov, V. K. Kornev, N. F. Pedersen, *Physica C* **435**, 114 (2006).
21. N. V. Klenov, N. G. Pugach, A. V. Sharafiev, S. V. Bakurskiy and V. K. Kornev, *Physics of the Solid State* **52**, 2246 (2010).
22. I. Askerzade, *Low Temp. Phys.* **41**, 241 (2015).
23. A. Buzdin and A. E. Koshelev, *Phys. Rev. B* **67**, 220504(R) (2003).
24. N. G. Pugach, E. Goldobin, R. Kleiner, D. Koelle, *Phys. Rev. B.*, 81(10), 104513 (2010).
25. H. Sickinger, A. Lipman, M. Weides, R. G. Mints, H. Kohlstedt, D. Koelle, R. Kleiner, E. Goldobin, *Phys. Rev. Lett.* **109**, 107002 (2012).

26. E. Goldobin, H. Sickinger, M. Weides, N. Ruppelt, H. Kohlstedt, R. Kleiner, D. Koelle, *Appl. Phys. Lett.* **102**, 242602 (2013).
27. A. Lipman, R.G. Mints, R. Kleiner, D. Koelle, E. Goldobin, *Phys. Rev. B.* **90** (18), 184502 (2014).
28. R. Menditto, H. Sickinger, M. Weides, H. Kohlstedt, M. Zonda, T. Novotny, D. Koelle, R. Kleiner, E. Goldobin, *Phys. Rev. B.* **93**, 174506 (2016).
29. J. W. A. Robinson, S. Piano, G. Burnell, C. Bell, and M. G. Blamire, *Phys. Rev. Lett.* **97**, 177003 (2006).
30. S. Piano, J. W.A. Robinson, G. Burnell, M. G. Blamire *The European Physical Journal B* **58**, 123 (2007).
31. R. S. Keizer, S. T. B. Goennenwein, T. M. Klapwijk, G. Miao, G. Xiao, A. Gupta, *Nature* **439**, 825 (2006).
32. M. S. Anwar, M. Veldhorst, A. Brinkman, and J. Aarts, *Appl. Phys.Lett.* **100**, 052602 (2012).
33. V. Shelukhin, A. Tsukernik, M. Karpovski, Y. Blum, K. B. Efetov, A. F. Volkov, T. Champel, M. Eschrig, T. Lofwander, G. Schon, and A. Palevski, *Phys. Rev. B.* **73**, 174506 (2006).
34. A.K. Feofanov, V.A. Oboznov, V.V. Bol'ginov, et. al., *Nature Physics* **6**, 593 (2010).
35. R.G. Mints, *Phys. Rev. B* **57**, R3221 (1998).
36. J. Pfeiffer, M. Kemmler, D. Koelle, R. Kleiner, E. Goldobin, M. Weides, A. K. Feofanov, J. Lisenfeld, and A. V. Ustinov, *Phys. Rev. B.* **77**, 214506 (2008).
37. T. Golod, A. Iovan, V. M. Krasnov, *Nature communications* **6**, 8628 (2015).
38. I. V. Vernik, V. V. Bol'ginov, S. V. Bakurskiy, A. A. Golubov, M. Yu. Kupriyanov, V.V. Ryazanov and O. A. Mukhanov, *IEEE Trans. on Appl. Supercon.* **23** (3), 1701208, (2013).
39. S. V. Bakurskiy, N. V. Klenov, I. I. Soloviev, V. V. Bol'ginov, V. V. Ryazanov, I. I. Vernik, O. A. Mukhanov, M. Yu. Kupriyanov, and A. A. Golubov, *Appl. Phys. Lett.* **102**, 192603 (2013).
40. S. V. Bakurskiy, N. V. Klenov, I. I. Soloviev, M. Yu. Kupriyanov, A. A. Golubov, *Phys. Rev. B* **88**, 144519 (2013).
41. I. I. Soloviev, N. V. Klenov, S. V. Bakurskiy, V. V. Bol'ginov, V. V. Ryazanov, M. Y. Kupriyanov, and A. A. Golubov, *Appl. Phys. Lett.* **105**, 242601 (2014).
42. N. V. Klenov, V. I. Ruzhickiy, and I. I. Soloviev, *Moscow Univ. Phys. Bull.* **70**, 404 (2015).
43. M. Houzet, V. Vinokur, and F. Pistolesi, *Phys. Rev. B* **72**, 220506 (2005).
44. T. Yu. Karminskaya and M. Yu. Kupriyanov, *Pis'ma Zh. Eksp. Teor. Fiz.* **85**, 343 (2007) [*JETP Lett.* **85**, 286 (2007)].
45. T. Yu. Karminskaya, A. A. Golubov, M. Yu. Kupriyanov, and A. S. Sidorenko *Phys. Rev. B* **81**, 214518 (2010).
46. F. S. Bergeret, A. F. Volkov, and K. B. Efetov, *Phys. Rev. Lett.* **86**, 3140 (2001).
47. F. Born, M. Siegel, E. K. Hollmann, H. Braak, A. A. Golubov, D. Yu. Gusakova, and M. Yu. Kupriyanov, *Phys. Rev. B.* **74**, 140501 (2006).
48. A. A. Golubov, M. Yu. Kupriyanov, and Ya. V. Fominov, *JETP Lett.* **75**, 709 (2002) [*Pisma v ZhETF* **75**, 588 (2002)].
49. I. S. Burmistrov and N. M. Chtchelkatchev, *Phys. Rev. B* **72**, 144520 (2005).
50. S. V. Bakurskiy, N. V. Klenov, T. Yu. Karminskaya, M. Yu. Kupriyanov, and A. A. Golubov, *Supercond. Sci. Technol.* **26**, 015005 (2013).
51. R. S. Keizer, S. T. B. Goennenwein, T. M. Klapwijk, G. Miao, G. Xiao, A. Gupta, *Nature* **439**, 825 (2006).
52. S.V. Bakurskiy, N.V. Klenov, I.I. Soloviev, M.Yu Kupriyanov, and A.A. Golubov, *Appl. Phys. Lett.* , **108**,042602 (2016).

Dr. Sergey Bakurskiy

Researcher in the Lomonosov Moscow State University, Skobeltsyn
Institute of Nuclear Physics, 119991, Leninskie Gory, 1,
Moscow, Russia
e-mail: r3zz@mail.ru

Dr. Nikolay Klenov

Senior Researcher in the Lomonosov Moscow State University,
Skobeltsyn Institute of Nuclear Physics, 119991, Leninskie Gory, 1,
Moscow, Russia
e-mail: nvklenov@mail.ru

Dr. Igor Soloviev

Senior Researcher in the Lomonosov Moscow State University,
Skobeltsyn Institute of Nuclear Physics, 119991, Leninskie Gory, 1,
Moscow, Russia
e-mail: igor.soloviev@gmail.com

M.c. ASM, Prof. Dr. Anatoli Sidorenko

Director of Institute of Electronic Engineering and
Nanotechnologies AS RM
Academiei 3/3, Kishinev MD2028 Moldova
Tel 37322-737092; FAX 37322-727088
e-mail: anatoli.sidorenko@kit.edu
<http://nano.asm.md>

Prof. Dr. Mikhail Kupriyanov

Chief Researcher in the Lomonosov Moscow State University,
Skobeltsyn Institute of Nuclear Physics, 119991, Leninskie Gory, 1,
Moscow, Russia
e-mail: mkupr@pn.sinp.msu.ru

Prof. Dr. Alexander Golubov

Head of the laboratory in Moscow Institute of Physics and

Technology, State University, Institutsky pereulok, 9, Dolgoprudniy,
Moscow region, Russia

e-mail: A.A.Golubov@tnw.utwente.nl

Dr. Sergey Bakurskiy, Lomonosov Moscow State University, Skobeltsyn Institute of Nuclear Physics, 119991, Leninskie Gory, 1, Moscow, Russia, 74959392588, r3zz@mail.ru

Dr. Nikolay Klenov, Lomonosov Moscow State University, Skobeltsyn Institute of Nuclear Physics, 119991, Leninskie Gory, 1, Moscow, Russia, 74959392588, nvklenov@mail.ru

Dr. Igor Soloviev, Lomonosov Moscow State University, Skobeltsyn Institute of Nuclear Physics, 119991, Leninskie Gory, 1, Moscow, Russia, 74959392588, igor.soloviev@gmail.com

M.c. ASM, Prof. Dr. Anatoli Sidorenko, Institute of Electronic Engineering and Nanotechnologies AS RM Academiei 3/3, Kishinev MD2028 Moldova 37322-737092, anatoli.sidorenko@kit.edu

Prof. Dr. Mikhail Kupriyanov, Lomonosov Moscow State University, Skobeltsyn Institute of Nuclear Physics, 119991, Leninskie Gory, 1, Moscow, Russia, 74959392588, mkupr@pn.sinp.msu.ru

Prof. Dr. Alexander Golubov, Moscow Institute of Physics and Technology, State University, Institutsky pereulok, 9, Dolgoprudniy, Moscow region, Russia, 74954084554, A.A.Golubov@tnw.utwente.nl